Silver Chloride as a Heterogeneous Nucleant for the Growth of Silver Nanowires

Waynie M. Schuette and William E. Buhro*

Department of Chemistry, Washington University, Saint Louis, Missouri 63130-4899, United States

ABSTRACT Various additives are employed in the polyol synthesis of silver nanowires (Ag NWs), which are typically halide salts such as NaCl. A variety of mechanistic roles have been suggested for these additives. We now show that the early addition of NaCl in the polyol synthesis of Ag NWs from $AgNO_3$ in ethylene glycol results in the rapid formation of AgCl nanocubes, which induce the heterogeneous nucleation of metallic Ag upon their surfaces. Ag NWs subsequently grow from these nucleation sites. The conclusions are supported by studies using *ex situ* generated AgCl nanocubes.

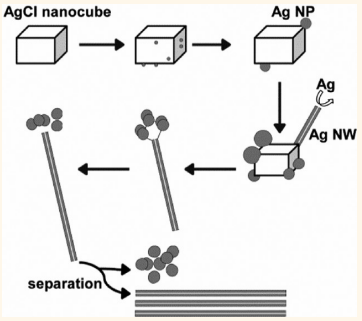

KEYWORDS: nucleation · nanowire · polyol · silver

Silver nanowires (Ag NWs) have received much interest in recent years due to their electronic and optical properties.[1−3] Straightforward, high-yield syntheses of one-dimensional Ag nanostructures are now available,[4−9] and Ag NWs are typically prepared by the polyol method.[10−23] Although much progress has been made on elucidating mechanistic aspects of the polyol synthesis of Ag NWs,[11,14−19,22,24] the role of the various additives employed remains unclear. In this paper, we show that the additive NaCl is rapidly converted to AgCl nanocubes under the conditions of the polyol synthesis. The AgCl nanocubes subsequently induce heterogeneous nucleation of metallic silver on their surfaces, initiating growth of Ag NWs. A detailed understanding of this heterogeneous-nucleation process may ultimately lead to rational control of Ag-NW diameters, diameter distributions, and aspect ratios.

To our knowledge, the first polyol synthesis of Ag NWs was reported by Xia and coworkers.[11] In this method, silver nitrate is titrated into a mixture of hot (150−180 °C) ethylene glycol and polyvinylpyrolidone (PVP). The ethylene glycol serves as both the solvent and reducing agent, and PVP as the surfactant.[24] Various additives, such as $PtCl_2$,[11,13,15,18] AgCl,[28] NaCl,[18,20,22,23,25−27] AgBr,[29] *etc.*, are also commonly employed and found to be crucial to the selective formation of NWs.[22] In some studies, initial reduction of the additives to homogeneous (Ag)[10,12] or heterogeneous (*e.g.*, Pt)[11,13,15,17] seeds were proposed, which subsequently promoted the growth (on Ag seeds) or heterogeneous nucleation (on Pt seeds) of the Ag NWs.

Other studies claim that the halide component of the above additives is the species that controls Ag-nanoparticle morphologies. In some, chloride ion is shown to selectively etch away multiply twinned Ag particles in the presence of oxygen,[19,25,26,30] which is proposed to hinder,[25] or, conversely, to promote[20] Ag NW formation. The equilibrium reaction of Ag^+ and Cl^- (from NaCl) to form AgCl has been proposed to buffer the Ag^+-ion concentration, limiting Ag nucleation events and thereby promoting the growth of Ag NWs.[20,21] Adsorption of Cl^- ions to Ag nanoparticle surfaces has also been proposed to provide electrostatic stabilization, preventing nanoparticle agglomeration and promoting Ag-NW growth.[7,14,19,25,26,30] In two studies, AgCl nanoparticles have been referred to as "seeds," but the precise role of

* Address correspondence to buhro@wustl.edu.

Received for review September 14, 2012 and accepted April 4, 2013.

Published online April 08, 2013
10.1021/nn400414h

the seeds was left unclear. To date, a heterogeneous-nucleation pathway involving AgCl nanoparticles has not been elucidated. Clearly, a mechanistic study that conclusively identifies the function of a NW-growth-promoting additive is desirable, given the wide variety of roles that have been proposed.

In this study, we monitored the polyol synthesis of Ag NWs employing NaCl as the growth-promoting additive. A combination of spectroscopy, microscopy, and X-ray diffraction (XRD) allowed us to determine the sequence of chemical, nucleation, and growth events occurring in the process. The detailed pathway was elucidated, which features the heterogeneous nucleation of Ag on *in situ* generated AgCl nanocubes as a prominent event. Control experiments were also conducted to establish this heterogeneous nucleation as the origin of the Ag NWs produced. An analogy to photographic processing using silver halide emulsions, and insights into optimizing Ag-NW growth are also discussed.

RESULTS

Description of the Synthetic Process. As in previous studies,[18,20,22,23,25−27] NaCl was used to promote Ag-NW growth in the polyol synthesis. In a typical procedure employing a comparatively large initial concentration of NaCl (24 mM), a solution of PVP in ethylene glycol was heated to 180 °C prior to addition of NaCl. Equimolar quantities of NaCl and $AgNO_3$ were then added to the hot solution, resulting in the instantaneous formation of a white precipitate. XRD patterns (Figure 1a,b) obtained from aliquots of the mixture established the precipitate to be AgCl, as has been previously demonstrated.[18,20−22,27]

The mixture was then stirred at 180 °C for 30 min, which was found empirically to maximize the eventual yield of Ag NWs. During this period the color of the mixture turned from white to a creamy yellow, which gradually darkened. XRD patterns of aliquots taken at various times evidenced the formation of small amounts of metallic Ag (Figure 1a,b). Spectroscopic monitoring by UV−visible spectroscopy revealed the emergence of the plasmon feature for metallic Ag at a wavelength of 435 nm after 6 min (Figure 2), which blue-shifted with time (435−402 nm).

Dropwise addition of a $AgNO_3$ solution was then initiated. A series of color changes ensued. The mixture became an olive color after about 10 min, and light brown after about 12 min. Silver-gray opalescent swirls appeared in the mixture after about 20 min, which indicated the formation of Ag NWs as established by SEM imaging (Figure 3b). The NWs were revealed to be pentagonally twinned in higher-magnification images (Figure S1), as has been previously reported.[24] The remainder of the $AgNO_3$ solution, if any, was added at a faster rate at this stage.

Trials in which Ag-NW formation was observed prior to the completion of $AgNO_3$ addition were typically

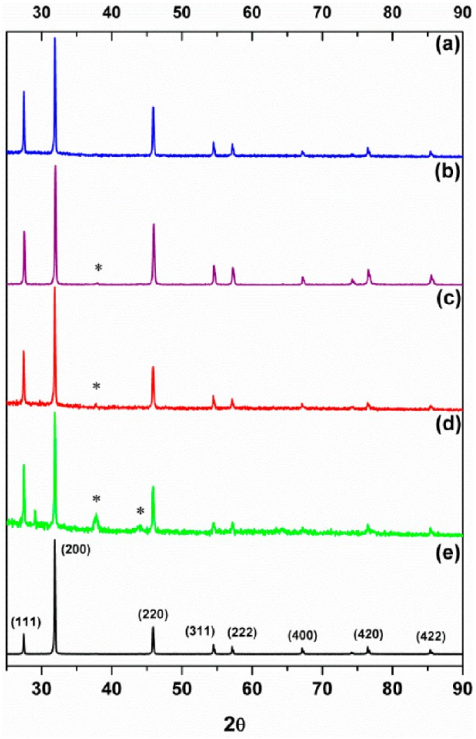

Figure 1. XRD patterns of an aliquot taken from reaction with (a) high NaCl concentration 1 min after initial addition of NaCl and $AgNO_3$ (blue), (b) high NaCl concentration 25 min after initial addition of NaCl and $AgNO_3$ (purple), (c) low NaCl concentration 1 min after initial addition of NaCl and $AgNO_3$ (red) and (d) low NaCl concentration 25 min after initial addition of NaCl and $AgNO_3$ (green). (e) XRD pattern of presynthesized AgCl nanocubes (black). Asterisks identify reflections from metallic Ag.

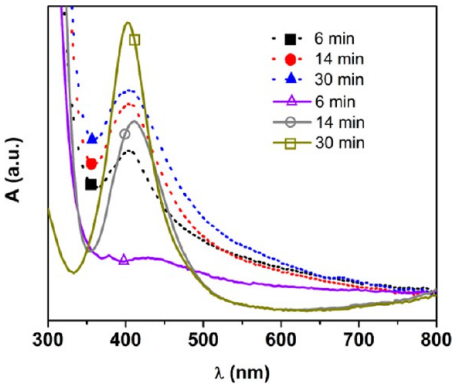

Figure 2. UV−visible spectra of aliquots removed from reaction mixtures at various times. The solid curves correspond to a high NaCl concentration experiment, and the dashed curves to a low NaCl concentration experiment.

accompanied by the formation of a lump of precipitate that was visually distinct from the dispersion of Ag NWs. Analysis of the lump material showed it to contain a vanishingly small amount of PVP, and to consist of AgCl (61.3 ± 0.7 mol %) intermixed with a smaller amount of metallic Ag (38.7 ± 0.7 mol %; see the Experimental Section). Predictably, the yield of Ag NWs was decreased by this byproduct-lump formation (see text below and Table 1).

The procedure was also conducted using a smaller initial concentration of NaCl (1.1 mM). In this case a white AgCl precipitate was not evident upon addition of equimolar quantities of NaCl and $AgNO_3$ to the PVP solution at 180 °C. Instead, a clear yellow solution formed. To establish the presence or absence of AgCl, the reaction was discontinued in two trials during the 30-min stirring period. After the reaction mixtures cooled, acetone was added, resulting in dark precipitates. XRD patterns of these precipitates (Figure 1c,d) established the presence of AgCl as the dominant phase, with smaller amounts of metallic Ag. The reaction, when continued as described above for the high-NaCl-concentration procedure, underwent a similar series of color changes upon further addition of $AgNO_3$. SEM images (Figure 3a) established the formation of Ag NWs as above.

Elemental analysis of a representative Ag-NW product showed that it contained no detectable PVP, establishing its removal in the workup procedure.

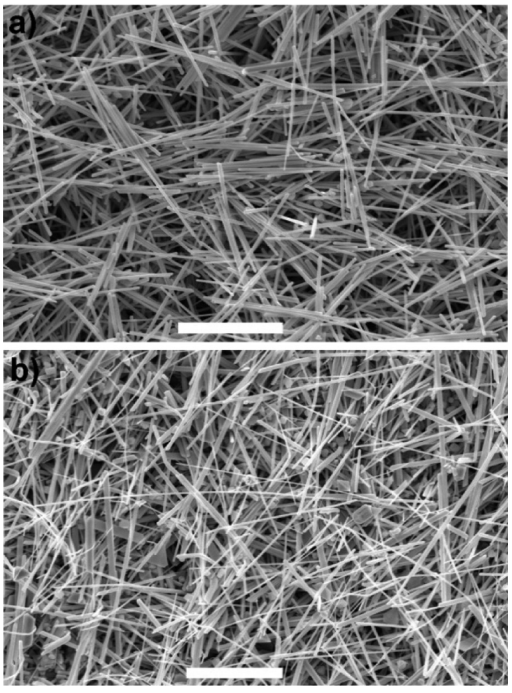

Figure 3. SEM images of purified wires synthesized with (a) low NaCl concentration, (b) high NaCl concentration. The scale bars are 10 μm.

XRD analyses revealed that the Ag NWs contained varying amounts of residual AgCl, which scaled with the initial concentration of NaCl and the successful separation of the byproduct lump (if any). Syntheses employing a low initial NaCl concentration gave Ag-NW product yields of up to 93%, with a AgCl contamination of <1% (Table 1). In contrast, syntheses employing a high initial NaCl concentration gave lower Ag-NW product yields of 40−60%, with a AgCl contamination as high as 24% (Table 1). Lump formation was much less common in trials conducted at low initial NaCl concentration. The residual AgCl was removed by washing the Ag-NW product with aqueous NH_4OH, as confirmed by XRD (Figure S2). An SEM image of washed material confirmed that the Ag NWs were unaffected (Figure S3).

Reaction Monitoring by SEM and TEM. An aliquot from a reaction mixture was taken during the 30-min stirring period after addition of equimolar quantities of NaCl and $AgNO_3$ (high-concentration trial). SEM images revealed faceted nanocrystals having cuboidal, cuboctahedral, and related morphologies (Figure 4a). We surmised these nanocrystals to be composed of AgCl, which was the major phase found by XRD (Figure 1a, b). SEM images obtained from aliquots from a low-concentration trial at the same reaction stage also contained cuboidal and cuboctahedral nanocrystals (Figure 4b), although the size distribution was shifted toward smaller sizes.

SEM images of the nanocrystals harvested in situ were compared to those of independently synthesized AgCl nanocrystals[31] (XRD pattern in Figure 1e) to provide further verification of their identity. As shown in Figure 4c, the independently synthesized AgCl nanocrystals exhibited closely similar morphologies. Elemental analyses by energy-dispersive X-ray spectroscopy (EDS) found both Ag and Cl, although the ratios were unreliable due to the instability of the nanocrystals under the electron beam. Under irradiation, small nodules of metallic Ag were observed to form on the AgCl nanocrystals, as the Ag:Cl ratio continued to increase with irradiation time (Figure S4). This instability was further visualized by comparing regions in the images that had been rastered by the electron beam with regions that were minimally exposed. The exposed regions were visibly darker due to metallic-Ag formation (Figure S5).[31]

TABLE 1. Ag and AgCl Reaction Yields Based on AgCl Source and Concentration, and Ethylene Glycol Purity

concentration of AgCl (mM)	% yield Ag[a]	% yield AgCl[a]	reaction products	ethylene glycol used
1.1	92.7 ± 0.18	0.82 ± 0.13	Ag NWs (See Figure S8)	Aldrich[c]
24	41.2 ± 0.73	24.2 ± 0.55	Ag NWs and lump intermixed (See Figure S9)	Aldrich[c]
0.36[b]	87.9 ± 0.21	0.55 ± 0.16	Ag NWs and separate lump	Aldrich[c]
1.1	79.8 ± 0.23	0.82 ± 0.17	Ag NWs and separate lump	J. T. Baker[d]
24	56.9 ± 0.09	4.29 ± 0.06	Ag NWs and separate lump	J. T. Baker[d]

[a] The reaction yields of the products before washing with NH_4OH. [b] Using presynthesized AgCl nanocubes. [c] Ethylene glycol from Aldrich had no certificate of analysis. [d] The impurities listed in the ethylene glycol from J. T. Baker are as follows: Cl, max. 5 ppm; Fe, max. 0.200 ppm.

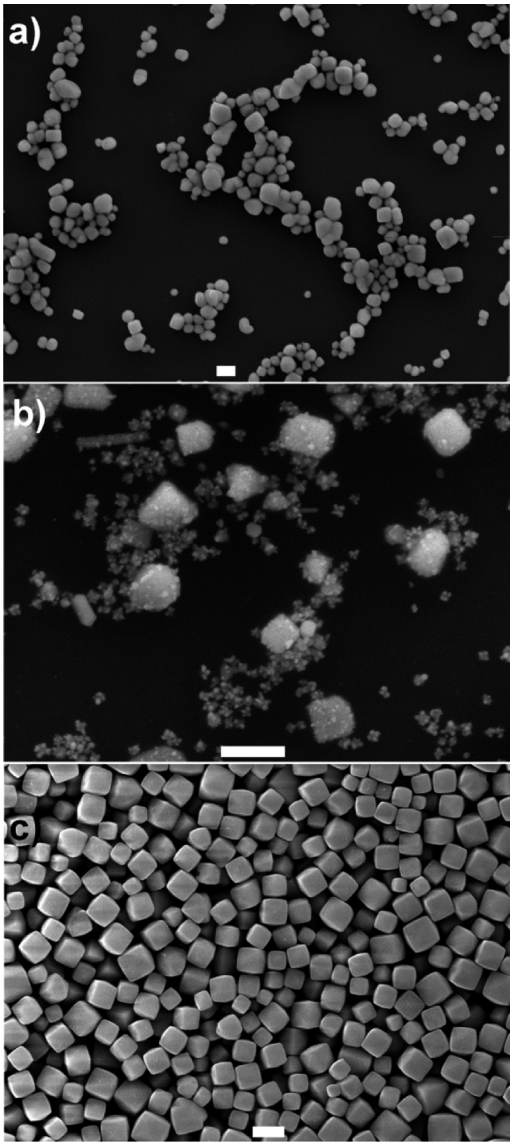

Figure 4. SEM images of (a) an aliquot removed from a high NaCl concentration reaction, (b) an aliquot removed from a low NaCl concentration reaction, and (c) independently synthesized AgCl nanocubes. The scale bars are 1 μm.

TEM imaging of the independently synthesized AgCl nanocrystals gave similar results. Electron-beam damage of the nanocubes ensued immediately upon beam focusing, resulting in metallic-Ag nanoparticle formation on the cube surfaces (Figure 5a). Thus, images of pristine AgCl nanocubes were difficult to obtain (as in Figure 4c). In certain specimens, synthesized at lower HCl concentrations,[31] filaments of metallic Ag were found to emanate from the AgCl cubes upon electron-beam exposure (Figure 5b), suggesting the initiation of NW growth. One can imagine such filaments developing into Ag NWs under reaction conditions (see below).

AgCl nanocubes harvested from a Ag-NW synthesis during the 30-min stirring period were also examined by TEM (Figure 5c,d). The images of the nanocubes

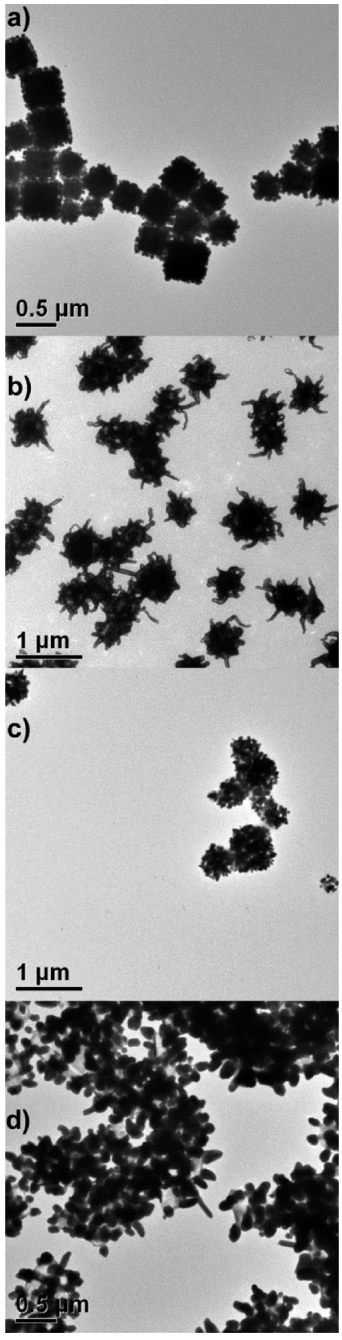

Figure 5. TEM images of nodules and filaments of Ag growing from AgCl cubes upon e-beam exposure; (a and b) independently synthesized AgCl cubes, (c and d) AgCl nanocubes from reaction mixtures employing added NaCl.

resembled those of the independently synthesized AgCl (Figure 5a,b), exhibiting Ag particles and filaments on the cube surfaces. As above, the majority of the Ag surface decoration formed upon beam exposure in the TEM. The XRD and UV–visible-spectroscopic monitoring experiments described above established some Ag formation during the 30-min stirring period. However, the resulting Ag nanostructures were obscured by the rapid Ag formation under the electron beam, and thus could not be imaged due to the extreme beam sensitivity of

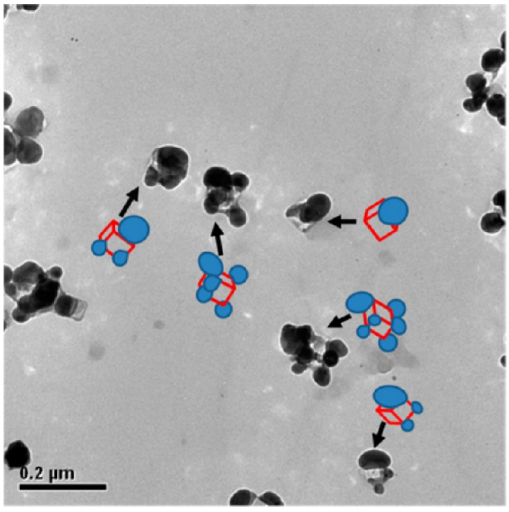

Figure 6. A TEM image of AgCl nanocubes generated in a reaction mixture employing added NaCl. The dark nodules decorating the nanocubes are Ag nanoparticles. In the inset cartoons, the AgCl nanocubes are depicted in red and the Ag nanoparticles in blue.

the AgCl nanocubes. Although direct evidence was therefore lacking, we presumed that the Ag initially formed under the reaction conditions was deposited on the surfaces of the AgCl nanocubes.

Another aliquot was taken from a low-NaCl-concentration Ag NW synthesis during the $AgNO_3$ dropwise-addition period, prior to the visual observation of silver-gray opalescent swirls indicative of extensive NW growth. A TEM image taken of the aliquot is shown in Figure 6. The image reveals comparatively large Ag nodules on the faces and vertices of the AgCl nanocubes. In Figure 6, the AgCl nanocubes appear to be colorless with gray patches, whereas the Ag nodules appear to be considerably darker. We have inserted cartoon representations into the Figure-6 image to assist the visualization of these nanostructures. As above, the majority of the Ag-nodule formation occurred in the microscope under e-beam exposure. However, the pattern of Ag-nodule decoration on the cubes presumably resulted from an underlying pattern of pre-existing Ag nuclei present on the cubes prior to beam exposure.

A related aliquot from a low-NaCl-concentration Ag NW synthesis was examined by SEM, prior to the visual observation of silver-gray opalescent swirls indicative of extensive NW growth (Figure 7). Small AgCl cubes with Ag-nodule decoration like those in Figure-6 TEM images were observed in the Figure-7 SEM images as well. Additionally, the Figure-7 SEM images clearly showed that short segments of Ag NWs were beginning to form. Careful inspection revealed that these NW segments were generally adhering to a AgCl nanocuboid, to which was also attached ≥ 4 Ag nanoparticles. Several such nanostructures are identified by arrows in Figure 7, and one is rendered in cartoon form

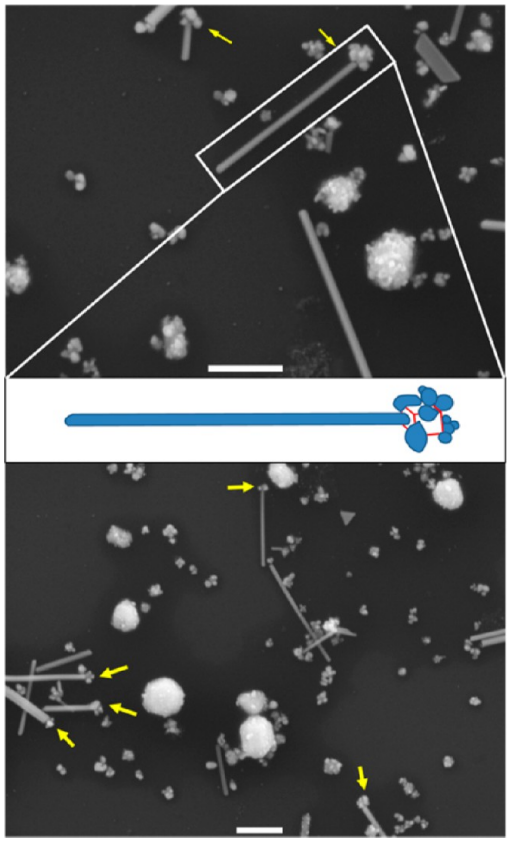

Figure 7. SEM images taken of an aliquot from a reaction mixture employing added NaCl (low-concentration trial). The aliquot was removed 5 min after the start of dropwise addition of $AgNO_3$ solution. The arrows mark Ag NWs emanating from AgCl nanocuboids (see text). One such nanostructure is depicted in cartoon form. The scale bars are 1 μm.

to aid in visualization. The results strongly suggested that Ag NW growth resulted from elongation of a Ag nodule formed on the AgCl nanocube at the earlier stage represented by the Ag-nodule-decorated nanocubes evident in both Figures 6 and 7. Generally, only a single Ag NW was found emanating from a nanocube cluster.

A related aliquot was taken from a high-NaCl-concentration Ag NW synthesis, 10 min after the stirring period, during the dropwise $AgNO_3$ addition, and prior to extensive NW growth. SEM images (Figure 8) revealed aggregated piles of large Ag nanoparticles, which in some cases appeared to be remnants of formerly cubic structures. Such pseudocubic piles apparently resulted from the reduction of large AgCl cubes to Ag particles. One or more Ag NWs were infrequently found to emanate from these nanoparticle piles, in a manner reminiscent of the clearer results in Figure 7.

Small AgCl nanocubes like those evident in Figure 7 were absent from images like those in Figure 8. Moreover, a reexamination of Figure 7 showed that the smaller AgCl nanocubes were more likely to nucleate

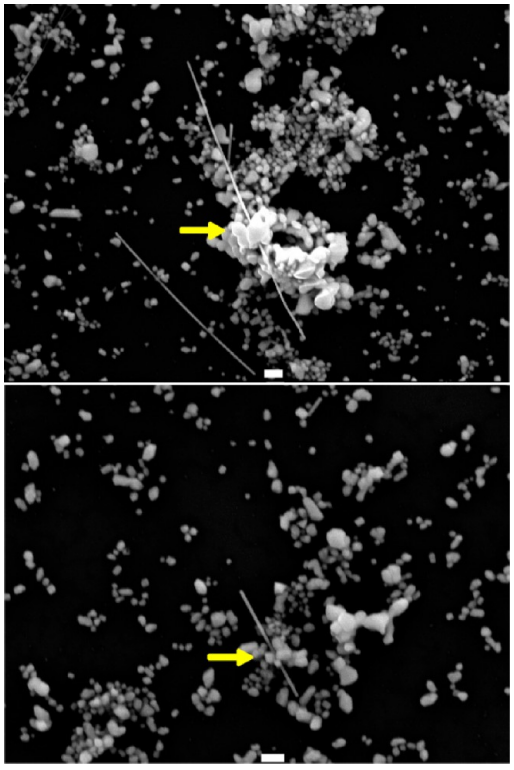

Figure 8. SEM images taken of an aliquot from a reaction mixture employing added NaCl (high-concentration trial). The aliquot was removed 10 min after the start of dropwise addition of $AgNO_3$ solution. The scale bars are 1 μm. The arrows identify piles of Ag nanoparticles that may be remnants of large AgCl nanocubes.

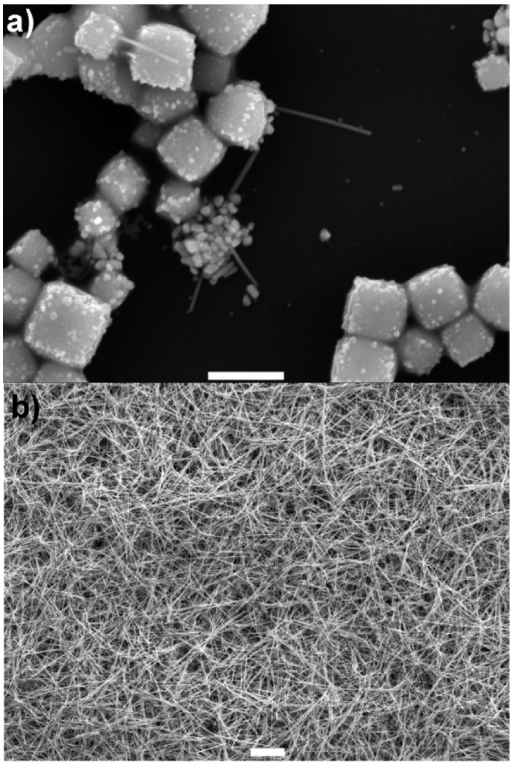

Figure 9. (a) SEM image taken of an aliquot from a reaction mixture employing presynthesized AgCl nanocubes. The aliquot was removed 23 min after the start of dropwise addition of $AgNO_3$ solution. The scale bar is 1 μm. (b) SEM image of purified Ag NWs obtained from a synthesis employing presynthesized AgCl nanocubes. The scale bar is 10 μm.

Ag NWs than were the larger AgCl nanocubes also evident in Figure 7. The results were consistent with the final NW images in Figure 3, which revealed that the low-NaCl-concentration synthesis was more selective for NW growth (Figure 3a). The high-NaCl-concentration synthesis (Figure 3b) contained a larger Ag nanoparticle fraction and a broader diameter distribution for the Ag NWs. Thus, the small AgCl nanocubes produced at low NaCl concentration were more-effective nucleating agents for Ag NW growth.

Ag NW Growth from Presynthesized AgCl Nanocubes. The results above suggested that the Ag NWs were nucleated by the AgCl nanocubes, or, more precisely, that they were grown from the Ag nanoparticles themselves heterogeneously nucleated upon the AgCl nanocubes. If so, then the direct addition of presynthesized AgCl nanocubes should be sufficient to induce NW growth, without the NaCl additive. Synthetic trials were conducted as above, with the addition of dispersions of presynthesized AgCl nanocubes (Figure 4c) in place of the initial, equimolar quantities of $AgNO_3$ and NaCl. Color changes and other experimental observations paralleled those described above.

An SEM image of an aliquot taken 23 min after the start of dropwise $AgNO_3$ addition is shown in Figure 9a. Ag NWs were observed to have grown from AgCl nanocube surfaces. An SEM image of the purified Ag NW product is shown in Figure 9b. The results established that AgCl nanocubes were necessary and sufficient for the growth of Ag NWs.

The yields of the Ag NWs grown with the presynthesized AgCl nanocubes approached 90%, and were thus comparable to the best yields obtained from low-NaCl-concentration trials (Table 1). The NWs were obtained with minimal AgCl contamination (Table 1). The quality of the product in selectivity for NW formation and diameter distribution (Figure 9b) was equal to or surpassed that achieved in the low-concentration-NaCl synthesis (Figure 3a).

Supporting Evidence for Heterogeneous Nucleation. If heterogeneous nucleation on AgCl nanocubes was the primary nucleation mechanism for Ag NWs, then, with a constant amount of $AgNO_3$ additive (after AgCl formation), the length of the Ag NWs should anticorrelate with the number of AgCl nanocubes present. Smaller numbers of AgCl nanocubes should on average produce longer wires. If one assumes that high initial AgCl concentrations produce larger numbers of AgCl nanocubes than do low initial AgCl concentrations, then the low NaCl-concentration trials should produce longer wires than do the high NaCl-concentration trials. This hypothesis was experimentally tested.

The Ag NW length distributions from representative high (blue) and low (red) NaCl-concentration trials are

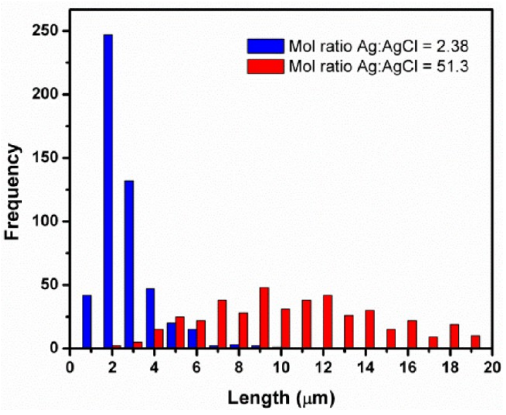

Figure 10. A histogram showing the dependence of Ag-NW length on the mole ratio of Ag to AgCl in the reaction mixture. The mole ratio of 2.38 corresponds to a high NaCl-concentration reaction and the mole ratio of 51.3 corresponds to a low NaCl-concentration reaction. The mean lengths were 2.2 μm $\pm$ 60% and 11.4 μm $\pm$ 50%, respectively.

plotted in Figure 10. These distributions were constructed using random length measurements obtained from SEM images. The measurements were collected from specimens having low NW-coverage densities such that individual NWs were readily discerned in the images. The mean NW length from the high-concentration trial was 2.2 μm with a standard deviation in the distribution of 1.3 μm, or 60% of the mean length. The mean length from the low-concentration trial was 11.4 μm with a standard deviation in the distribution of 5.7 μm, or 50% of the mean length. The low-concentration trial produced markedly longer mean Ag NW lengths, consistent with expectation for a primary heterogeneous-nucleation mechanism.

Control Experiments. Previous studies of the polyol synthesis of Ag NWs established that halide additives such as NaCl were essential to the selective formation of NWs rather than other Ag nanoparticle morphologies.[18,22] To confirm the necessity of added chloride (as NaCl) under our conditions, we conducted a control experiment (using Aldrich ethylene glycol) in which NaCl was omitted, but our other reaction parameters were unchanged. An SEM image of the resulting product established that selectivity for NW formation was lost (Figure S6a). Instead, a complex mixture of nanoparticle morphologies was observed with a very small proportion of Ag NWs, which were comparatively short. Thus, NaCl addition was shown to be essential to NW selectivity under our conditions as well.

A second control experiment was conducted to examine the role of the second (dropwise) $AgNO_3$ addition. As detailed above, $AgNO_3$ was added in two fractions in our procedure. The initial addition with NaCl was to promote AgCl-nanocube formation, and the second addition was to promote Ag NW growth. However, one may note that AgCl contains Ag^+, and was therefore a potentially sufficient source to support NW growth, without the second addition of $AgNO_3$. A synthetic trial in which this second addition was omitted but our other reaction parameters were maintained (for high NaCl concentration) failed to produce Ag NWs (Figure S6b). The product contained a large fraction of AgCl nanocubes intermixed with various Ag-nanoparticle morphologies. The result established that the primary source of Ag^+ to support NW growth was the $AgNO_3$ added dropwise in the second fraction,[11] after AgCl-nanocube formation was complete.

Another control experiment demonstrated the importance of the 30-min stirring period after *in situ* generation of the AgCl nanocubes. As described above, the formation of small amounts of metallic Ag was observed during this period, as determined by XRD and absorption spectroscopy (Figures 1 and 2). We surmised that this Ag formed upon the surfaces of the AgCl nanocubes (see above), providing nucleation sites for subsequent NW growth. A trial in which the 30-min stirring period was omitted gave a mixture of Ag-nanoparticle morphologies without selectivity for NW growth (Figure S6c). The result suggested that the AgCl nanocubes were activated for NW growth by surface-Ag formation during the stirring period.

A final set of control experiments was conducted using high-purity ethylene glycol ($\leq$5 ppm Cl, $\leq$0.200 ppm Fe) from J. T. Baker for Ag NW growth. The reaction yields were similar to those from syntheses employing Aldrich ethylene glycol (Table 1). SEM images (Figure S7a,b) of the NWs showed comparable Ag-NW quality and selectivity to NWs grown in Aldrich ethylene glycol. Thus, our synthetic results were not significantly influenced by impurities that may have been present in the Aldrich ethylene glycol.

DISCUSSION

Four observations strongly indicate that the role of the NaCl additive is to generate AgCl nanocubes, which serve as heterogeneous nucleants for Ag NW growth. (1) Synthetic trials lacking a chloride additive, and therefore AgCl nanocubes, failed to give Ag NWs, producing Ag nanoparticles having other morphologies instead.[18,22] (2) AgCl nanocubes generated independently and added to the syntheses were active for nucleating Ag NWs, functioning in the same manner as the AgCl nanocubes generated *in situ* by NaCl addition. (3) Images of Ag NWs nucleated on and growing from AgCl nanocubes were obtained. (4) The lengths of the Ag NWs were anticorrelated with the quantity and presumed number density of AgCl nanocubes, as expected for a heterogeneous-nucleation mechanism. The heterogeneous-nucleation and growth process elucidated here is summarized in Scheme 1.

The Scheme 1 pathway bears close similarity to the photographic process employing silver-halide emulsions.[33,34] When silver-halide crystallites in the emulsions are exposed to light, mobile Ag^+ ions in the

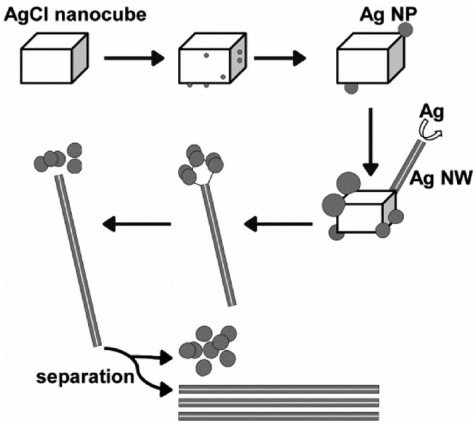

Scheme 1. Depiction of the heterogeneous nucleation and growth pathway for Ag NWs.

lattice are reduced by photogenerated electrons. Small Ag_n clusters are formed on the crystallite surfaces, which constitute the (invisible) latent image. At the same time, the photogenerated holes convert halide ions to dihalogen. The latent image is developed by treating the exposed emulsion to a reducing agent. The Ag_n clusters catalyze the complete reduction of the exposed AgX crystallites to metallic Ag. The critical, developable cluster size is believed to be Ag_4, such that the unexposed AgX crystallites are not reduced in development, and remain unreacted. The resulting distribution of metallic Ag particles within the AgX emulsion forms the photographic image.

In the present work, addition of NaCl and $AgNO_3$ to the polymer solution results in the immediate formation of AgCl nanocubes. These are generated in hot ethylene glycol, which is the reductant, and small Ag_n clusters and nanoparticles are formed on the nanocube surfaces during the subsequent stirring period (Scheme 1). These clusters and nanoparticles may be "developed" by exposure to an electron beam in a microscope, or by continued reduction under the reaction conditions. Several large Ag nanoparticles typically form on each AgCl nanocube. Some of these Ag nanoparticles become pentagonally twinned. Such twinned nanoparticles were previously shown to grow anisotropically into pentagonally twinned NWs by addition of Ag to the remote tip.[24] Although both the added $AgNO_3$ and the AgCl nanocubes are sources of Ag^+ to feed the reduction process, the second, dropwise addition of $AgNO_3$ is primarily responsible for NW growth. Even so, the AgCl nanocubes become degraded and partially consumed by reduction, eventually releasing the attached Ag NWs and nanoparticles. The NWs and nanoparticles are separated in the workup procedure.

CONCLUSIONS

In summary, the role of the NaCl additive, and by analogy other alkali halide additives that have also been employed in polyol Ag NW syntheses, is to generate heterogeneous nucleants in the form of Ag-halide nanocubes. The results reported here establish that the smaller AgCl nanocubes are more-potent heterogeneous nucleants that afford higher selectivity for Ag NW growth and narrower NW diameter distributions. Consequently, improved synthetic control might be achieved by the use of small, presynthesized AgCl nanocubes rather than those generated *in situ* from chloride additives. Efforts are currently underway in our laboratory to determine which reaction parameters may be varied to control Ag NW mean diameter and length.

EXPERIMENTAL SECTION

General Methods. All syntheses were conducted under ambient conditions. Anhydrous ethylene glycol (99.8%, Aldrich), ethylene glycol (>99.0%, J. T. Baker), $AgNO_3$ (99+%, Aldrich), polyvinylpyrrolidone (PVP, MW ≈ 55 000, Aldrich), sodium chloride (99+%, Aldrich), ammonium hydroxide (28.0−30.0 w/w %, Fisher Scientific), and acetone (reagent grade, Aldrich) were used as received without further purification. Si(111) wafers were purchased from Aldrich. Deionized water was used in all procedures.

AgCl nanocubes were prepared according to a previously reported method.[31] The white precipitate obtained from the synthesis[31] was then washed with water and acetone to remove the excess ethylene glycol and PVP, and was then vacuum-dried for 3−4 h. The overall reaction yield varied from 27 to 67%. The AgCl nanocubes were then suspended in 5 mL of ethylene glycol. The resulting stock AgCl dispersions were generally used within a week of preparation.

SEM images were collected using a JEOL 7001LVF FE-SEM with an acceleration voltage of 15 kV. TEM images were collected using a JEOL 2000 FX microscope with an acceleration voltage of 200 kV. To prepare SEM samples, a few drops of the purified product (diluted in water) were drop casted onto the Si(111) wafer and air-dried. To prepare the TEM samples, TEM grids (copper, coated with holey carbon film, from Ted Pella) were dipped into the reaction solution or purified Ag NWs (diluted in water) and air-dried.

XRD patterns were collected on Rigaku DmaxA diffractometer using Cu Kα radiation (λ = 1.541 845 Å) and Materials Data, Inc. (MDI) software, and were processed using the JADE software package. To prepare the XRD samples, a few drops of a sample dispersion were drop casted onto the glass XRD sample holder and dried in the fume hood overnight. The process was repeated until a uniform layer was visible. Refinements of XRD data to quantify phase composition were performed using Powdercell 2.4 freeware.[32]

UV−visible spectra were acquired using a Varian Cary 100 Bio UV−visible spectrophotometer. Samples were prepared by adding 10 drops of the reaction mixture and 3 mL of water into a glass cuvette. Elemental analyses for C, H, and N were conducted by Galbraith Laboratories, Inc. (Knoxville, TN).

Synthesis of Silver Nanowires (Ag NWs). The procedure was adapted from a previously reported synthesis.[11] PVP (334 mg, 3.0 mmol) was dissolved in ethylene glycol (20 mL) and refluxed with stirring in an oil bath at 180 °C. The reaction mixture was maintained under these conditions for 5 min, and then varying amounts of NaCl and $AgNO_3$, or alternatively AgCl nanocubes, were added, as described below:

(a). High-Concentration Addition of NaCl and $AgNO_3$. Ethylene glycol solutions of NaCl (1.2 mL, 0.43 M) and $AgNO_3$ (1.2 mL, 0.43 M) were simultaneously injected into the stirring, hot

reaction mixture to achieve a final AgCl concentration of 24 mM. The procedure continues in part d below.

(b). Low-Concentration Addition of NaCl and $AgNO_3$. Ethylene glycol solutions of NaCl (50 μL, 0.43 M) and $AgNO_3$ (50 μL, 0.43 M) were simultaneously injected into the stirring, hot reaction mixture to achieve a final AgCl concentration of 1.1 mM. The procedure continues in part d below.

(c). Addition of Presynthesized AgCl Nanocubes. A stock dispersion of AgCl was sonicated for a few seconds prior to use. An aliquot was removed from the dispersion (0.5 mL, 0.2−0.4 M) of AgCl) and injected into the stirring, hot reaction mixture to achieve a final AgCl concentration of 4.8−9.8 mM. The procedure continues in part d below.

(d). Growth and Purification of Ag NWs. The reaction mixture obtained from part a, b, or c above was refluxed for an additional 25 min with stirring. Then, a $AgNO_3$ solution (10 mL, 0.12 M) was added dropwise at a rate of 25 mL/h while maintaining reflux and stirring. Silver-gray opalescent swirls of precipitate were observed within 15−20 min of the addition period, indicative of Ag NW formation. At that point, the addition rate was increased to complete addition within 1 min. The mixture was then refluxed for an additional 15 min.

The reaction mixture was allowed to cool to room temperature. H_2O (100 mL) was added to the mixture. Fractions of the mixture (10−12 mL) were successively removed and centrifuged on a benchtop unit. The precipitated Ag NWs were collected and combined, and the yellow supernatant fractions were discarded. The mass yield was recorded, and analyzed as described below.

(e). Yield and Characterization of Ag NWs. Elemental analysis of a representative Ag-NW specimen from the synthetic procedures above revealed a negligible amount of residual organics (C, <0.5%; H, <0.5%; N, <0.5%), indicating that the PVP was removed by the workup procedure (part d, above). XRD patterns of Ag NWs showed reflections from both Ag and AgCl (Figures S8 and S9), in relative amounts that varied with the synthetic procedure. The XRD data were refined to quantify the Ag and AgCl volume fractions. The refinements produced fitted sum patterns (Figures S8, S9) and the volume percentages of Ag and AgCl in the specimens. Three separate refinement runs were performed on each XRD pattern analyzed, and the results were averaged. These values were used with the recorded product masses to provide the percent yields reported in Table 1.

The residual AgCl in the specimens was removed by the following procedure. A Ag-NW product was redispersed in water (5 mL) and aqueous NH_4OH (2 mL, 28.0−30.0 w/w %) was added to the dispersion. The dispersion was shaken and then centrifuged. The precipitated Ag NWs were collected and the supernatant was discarded. XRD patterns (Figure S2) obtained of the Ag NWs after this wash confirmed the removal of AgCl.

Trials in which the dropwise addition of the $AgNO_3$ solution was incomplete when the formation of Ag NWs was observed (by visualization of gray opalescent swirls) resulted in the formation of a solid lump of byproduct. In some cases, this lump was sufficiently large (0.3−1.0 cm diameter) to be easily manually separated from the Ag NWs, while in other cases, it broke up into smaller pieces and became intermixed with the Ag NWs. Trials in which the dropwise addition of the $AgNO_3$ solution was completed before the Ag NW growth was observed did not produce such a byproduct lump. Elemental analysis of a representative lump revealed small amounts of residual organics (C, 1.36%; H, <0.5%; N, <0.5%). An XRD pattern (Figure S10) of the lump showed it to be a mixture of AgCl (80.4 vol %) and Ag (19.6 vol %). As shown in Table 1, the trials that did not produce a lump had higher yields of Ag NWs. Additionally, the amount of residual AgCl in the Ag-NW product was lower in reactions that had a separable lump. Trials employing a lower initial NaCl concentration also produced a lower yield of AgCl, and a higher yield of Ag NWs.

Conflict of Interest: The authors declare no competing financial interest.

Acknowledgment. We thank Dr. Fudong Wang (Washington U.) for helpful discussions and experimental advice. We are also grateful to Prof. Patrick Gibbons (Washington U.), Dr. Tyrone Daulton (Washington U.), and Dr. Paul Carpenter (Washington U.) for assistance with TEM, SEM, and XRD. This work was supported by the NSF (CHE-1012898).

Supporting Information Available: Additional SEM images of pentagonally twinned Ag NWs, Ag NWs after NH_4OH purification and from various control reactions, XRD patterns of Ag NWs from various reactions, side products and after NH_4OH purification and SEM images and EDS data of electron-beam-damaged AgCl nanocrystals. This information is available free of charge *via* the Internet at http://pubs.acs.org.

REFERENCES AND NOTES

1. Wiley, B. J.; Im, S. H.; Li, Z. −Y.; McLellan, J.; Siekkinen, A.; Xia, Y. Maneuvering the Surface Plasmon Resonance of Silver Nanostructures through Shape-Controlled Synthesis. *J. Phys. Chem. B* **2006**, *110*, 15666–15675.
2. Kelly, K. L.; Coronado, E.; Zhao, L. L.; Schatz, G. C. The Optical Properties of Metal Nanoparticles: The Influence of Size, Shape and Dielectric Environment. *J. Phys. Chem. B* **2003**, *107*, 668–677.
3. Amendola, V.; Bakr, O. M.; Stellacci, F. A Study of the Surface Plasmon Resonance of Silver Nanoparticles by the Discrete Dipole Approximation Method: Effect of Shape, Size, Structure and Assembly. *Plasmonics* **2010**, *5*, 85–97.
4. Zou, K.; Zhang, X. H.; Duan, X. F.; Meng, X. M.; Wu, S. K. Seed-Mediated Synthesis of Silver Nanostructures and Polymer/Silver Nanocables by UV Irradiation. *J. Cryst. Growth* **2004**, *273*, 285–291.
5. Sun, J.; Zhang, J.; Liu, W.; Liu, S.; Sun, H.; Jiang, K.; Li, Q.; Guo, J. Shape Controlled Synthesis of Silver Nanostructures. *Nanotechnology* **2005**, *16*, 2412–2414.
6. Wiley, B.; Sun, Y.; Mayers, B.; Xia, Y. Shape Controlled Synthesis of Metal Nanostructures: The Case of Silver. *Chem.—Eur. J.* **2005**, *11*, 454–463.
7. Wiley, B.; Sun, Y.; Xia, Y. Synthesis of Silver Nanostructures with Controlled Shapes and Properties. *Acc. Chem. Res.* **2007**, *40*, 1067–1076.
8. Samanta, S.; Pyne, S.; Sarkar, P.; Sahoo, G. P.; Bar, H.; Bhui, D. K.; Misra, A. Synthesis of Silver Nanostructures of Varying Morphologies through Seed Mediated Growth Approach. *J. Mol. Liq.* **2010**, *153*, 170–173.
9. Chen, D.; Qiao, X.; Chen, J. Morphology-Controlled Synthesis of Silver Nanostructures *via* a Solvothermal Method. *J. Mater. Sci.: Mater. Electron.* **2011**, *22*, 1335–1339.
10. Sun, Y.; Xia, Y. Large-Scale Synthesis of Uniform Silver Nanowires through a Soft, Self-Seeding, Polyol Process. *Adv. Mater.* **2002**, *14*, 833–837.
11. Sun, Y.; Yin, Y.; Mayers, B. T.; Herricks, T.; Xia, Y. Uniform Silver Nanowires Synthesis by Reducing $AgNO_3$ with Ethylene Glycol in the Presence of Seeds and Poly(vinyl pyrrolidone). *Chem. Mater.* **2002**, *14*, 4736–4745.
12. Gao, Y.; Jiang, P.; Liu, D. F.; Yuan, H. J.; Yan, X. Q.; Zhou, Z. P.; Wang, J. X.; Song, L.; Liu, L. F.; Zhou, W. Y.; et al. Synthesis, Characterization and Self-Assembly of Silver Nanowires. *Chem. Phys. Lett.* **2003**, *380*, 146–149.
13. Tsuji, M.; Nishizawa, Y.; Hashimoto, M.; Tsuji, T. Syntheses of Silver Nanofilms, Nanorods, and Nanowires by a Microwave-Polyol Method in the Presence of Pt Seeds and Polyvinylpyrrolidone. *Chem. Lett.* **2004**, *33*, 370–371.
14. Wiley, B.; Sun, Y.; Xia, Y. Polyol Synthesis of Silver Nanostructures: Control of Product Morphology with Fe(II) or Fe(III) Species. *Langmuir* **2005**, *21*, 8077–8088.
15. Gao, Y.; Jiang, P.; Song, L.; Liu, L.; Yan, X.; Zhou, Z.; Liu, D.; Wang, J.; Yuan, H.; Zhang, Z.; et al. Growth Mechanism of Silver Nanowires Synthesized by Polyvinylpyrrolidone-Assisted Polyol Reduction. *J. Phys. D: Appl. Phys.* **2005**, *38*, 1061–1067.
16. Chen, C.; Wang, L.; Jiang, G.; Yang, Q.; Wang, J.; Yu, H.; Chen, T.; Wang, C.; Chen, X. The Influence of Seeding Conditions and Shielding Gas Atmosphere on the Synthesis of Silver Nanowires through the Polyol Process. *Nanotechnology* **2006**, *17*, 466–474.

17. Chen, C.; Wang, L.; Jiang, G.; Zhou, J.; Chen, X.; Yu, H.; Yang, Q. Study on the Synthesis of Silver Nanowires with Adjustable Diameters through the Polyol Process. *Nanotechnology* **2006**, *17*, 3933–3938.
18. Tsuji, M.; Matsumoto, K.; Jiang, P.; Matsuo, R.; Tang, X.-L.; Kamarudin, K. S. N. Roles of Pt Seeds and Chloride Anions in the Preparation of Silver Nanorods and Nanowires by Microwave Polyol Method. *Colloids Surf., A* **2008**, *316*, 266–277.
19. Korte, K. E.; Skrabalak, S. E.; Xia, Y. Rapid Synthesis of Silver Nanowires through a CuCl- $CuCl_2$ Mediated Polyol Process. *J. Mater. Chem.* **2008**, *18*, 437–441.
20. Gou, L.; Chipara, M.; Zaleski, J. M. Convenient Rapid Synthesis of Silver Nanowires. *Chem. Mater.* **2007**, *19*, 1755–1760.
21. Li, Z. C.; Shang, T. M.; Zhou, Q. F.; Feng, K. Sodium Chloride Assisted Synthesis of Silver Nanowires. *Micro Nano Lett.* **2011**, *6*, 90–93.
22. Coskun, S.; Aksoy, B.; Unalan, H. E. Polyol Synthesis of Silver Nanowires: An Extensive Parametric Study. *Cryst. Growth Des.* **2011**, *11*, 4963–4969.
23. Lin, H.; Ohta, T.; Paul, A.; Hutchison, J. A.; Demid, K.; Lebedev, O.; Tendeloo, G. V.; Hofkens, J.; Uji-i, H. Light-Assisted Nucleation of Silver Nanowires during Polyol Synthesis. *J. Photochem. Photobiol., A* **2011**, *221*, 220–223.
24. Sun, Y.; Mayers, B.; Herricks, T.; Xia, Y. Polyol Synthesis of Uniform Silver Nanowires: A Plausible Growth Mechanism and the Supporting Evidence. *Nano Lett.* **2003**, *3*, 955–960.
25. Wiley, B.; Herricks, T.; Sun, Y.; Xia, Y. Polyol Synthesis of Silver Nanoparticles: Use of Chloride and Oxygen To Promote the Formation of Single-Crystal, Truncated Cubes and Tetrahedrons. *Nano Lett.* **2004**, *4*, 1733–1739.
26. Wiley, B.; Sun, Y.; Xia, Y. Synthesis of Silver Nanostructures with Controlled Shapes and Properties. *Acc. Chem. Res.* **2007**, *40*, 1067–1076.
27. Zhang, W. C.; Wu, X. L.; Chen, H. T.; Gao, Y. J.; Zhu, J.; Huang, G. S.; Chu, P. K. Self- Organized Formation of Silver Nanowires, Nanocubes and Bipyramids *via* a Solvothermal Method. *Acta Mater.* **2008**, *56*, 2508–2513.
28. Hu, L.; Kim, H. S.; Lee, J.-Y.; Peumans, P.; Cui, Y. Scalable Coating and Properties of Transparent, Flexible, Silver Nanowire Electrodes. *ACS Nano* **2010**, *4*, 2955–2963.
29. Liu, S.; Yue, J.; Gedanken, A. Synthesis of Long Silver Nanowires from AgBr Nanocrystals. *Adv. Mater.* **2001**, *13*, 656–659.
30. Im, S. H.; Lee, Y. T.; Wiley, B.; Xia, Y. Large Scale Synthesis of Silver Nanocubes: The Role of HCl in Promoting Cube Perfection and Monodispersity. *Angew. Chem., Int. Ed.* **2005**, *44*, 2154–2157.
31. Kim, S.; Chung, H.; Kwon, J. H.; Yoon, H. G.; Kim, W. Facile Synthesis of Silver Chloride Nanocubes and their Derivatives. *Bull. Korean Chem. Soc.* **2010**, *31*, 2918–2922.
32. Kraus, W.; Nolze, G. *POWDER CELL*—A Program for the Representation and Manipulation of Crystal Structures and Calculation of the Resulting X-Ray Powder Patterns. *J. Appl. Crystallogr.* **1996**, *29*, 301–303.
33. James, T. H. The Theory of the Photographic Process. *Mechanism of Formation of the Latent Image*; Hamilton, J. F., Ed.; Macmillan Publishing Co. Inc.: New York, 1977; pp 105−133.
34. Hamilton, J. F. The Silver Halide Photographic Process. *Adv. Phys.* **1988**, *37*, 359–441.